

See discussions, stats, and author profiles for this publication at: <https://www.researchgate.net/publication/271910535>

# Formation Mechanisms of GaN Nanowires Grown by Selective Area Growth Homoepitaxy

ARTICLE *in* NANO LETTERS · JANUARY 2015

Impact Factor: 13.59 · DOI: 10.1021/nl504099s

---

CITATIONS

4

READS

40

3 AUTHORS, INCLUDING:



Ž. Gacevic

Universidad Politécnica de Madrid

28 PUBLICATIONS 160 CITATIONS

SEE PROFILE

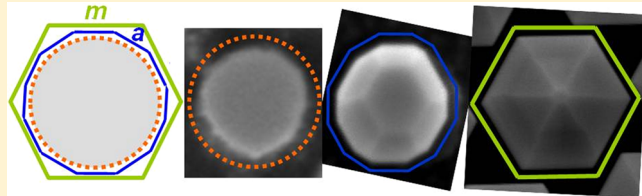
# Formation Mechanisms of GaN Nanowires Grown by Selective Area Growth Homoepitaxy

Žarko Gačević,\* Daniel Gómez Sánchez, and Enrique Calleja

ISOM - ETSIT, Universidad Politécnica de Madrid Avda. Complutense s/n, 28040 Madrid, Spain

**ABSTRACT:** This work provides experimental evidence and theoretical explanations regarding the formation mechanisms of GaN nanowires grown by selective area growth on GaN-on-sapphire templates. The first growth stage, driven by selective area growth kinetics, consists of initial nucleation (along the nanohole inner periphery), coalescence onset and full coalescence, producing a single nanocrystal within each nanohole. In the second growth stage, driven by free-surface-energy minimization, the formed nanocrystal undergoes morphological evolution, exhibiting initial cylindrical-like shape, intermediate dodecagonal shape and a final, thermodynamically stable hexagonal shape. From this point on, the nanowire vertical growth proceeds while keeping the stable hexagonal form.

**KEYWORDS:** GaN nanowires, molecular beam epitaxy, selective area growth, formation mechanism, morphological evolution



The potential of GaN nanowires (NWs) was recognized in the late 1990s, when several groups reported their self-assembled (SA) growth and their supreme crystal quality.<sup>1,2</sup> The SA growth however is characterized by intrinsically high randomness, which limits the control of epitaxial growth and further planar device processing. To allow for precise control of NWs' position, orientation (tilt and twist), diameter, height and density, several groups reported homoepitaxial selective area growth (SAG) of GaN NWs on GaN templates.<sup>3–6</sup> This fabrication technique allows realization of (In)GaN based arrays of nanolight-emitting diodes,<sup>7</sup> single photon sources,<sup>8</sup> photonic crystals,<sup>9</sup> and nanofield effect transistors.<sup>10</sup>

The lack of central symmetry of the wurtzite crystal leads to a strong anisotropy of III-nitrides' physical properties. Anisotropy of free surface energy, for example, leads to different growth rates along different crystal directions, being the critical issue for controlled nanostructure fabrication.<sup>11–13</sup> It determines the fabrication of a wide variety of zero-dimensional (0D), one-dimensional (1D), or two-dimensional (2D) III-N nanostructures, for which GaN NWs are an excellent "crystal platform".<sup>8,14–20</sup> The full exploitation of GaN NWs as carriers of III-N nanostructures requires a full understanding of the growth mechanisms that govern their initial nucleation and their posterior evolution into thermodynamically stable crystal objects. Recently, the formation mechanisms for SA GaN NWs have been reported for SA NWs grown on thin amorphous SiN and AlN buffer on Si(111).<sup>21</sup> The authors reported that on both substrates initial GaN self-nucleation occurs in the form of a spherical cap (a result of heteroepitaxial growth), which in later growth stages evolves into a thermodynamically stable hexagonal NW. In contrast, for SAG GaN NWs the nucleation steps and morphology evolution are determined by the homoepitaxial growth and by the fact that NWs diameter is fixed by the mask nanohole size. This work provides a detailed experimental evidence of the growth stages of SAG GaN NWs

and explains the driving mechanisms for their formation within the scopes of SAG kinetics and free-surface-energy minimization. A comparison of formation mechanisms and observed unstable crystal shapes for SA and SAG GaN NWs is also given.

The samples studied were grown in a RIBER Compact 21 Molecular Beam Epitaxy (MBE) system, equipped with a radio frequency plasma nitrogen source and two standard Knudsen cells for Ga. All growths were performed on ~3.3 μm thick commercial GaN-on-sapphire(0001) templates grown by metal organic vapor phase epitaxy. Prior to the MBE growth, a 7 nm thick TiN mask with nanoholes arranged in a compact hexagonal lattice (600 nm pitch and 500 nm diameter) was fabricated by colloidal lithography on the GaN templates.<sup>22</sup> For all samples (A–F) the Ga and N impinging fluxes and the growth temperature were kept constant ( $\Phi_{\text{Ga}} = 15 \text{ nm/min}$ ,  $\Phi_{\text{N}} = 4 \text{ nm/min}$  and  $T_g = 850^\circ\text{C}$ ) whereas the growth time was varied in the steps of  $t = 30, 60, 90, 120, 180$ , and 300 min. The samples morphological characterization was performed with a FEI Inspect F50 scanning electron microscope (SEM).

The SAG of GaN NWs can be divided into two growth stages. The first growth stage (I), driven by SAG kinetics,<sup>5</sup> consists of (i) initial "nucleation" of very small GaN islands (seeds), (ii) "coalescence onset", along the nanohole inner perimeter, and (iii) "full coalescence", that produces a single nanocrystal per nanohole, occupying most of its area. In the second growth stage (II), driven by free-surface-energy minimization,<sup>23</sup> the formed nanocrystal undergoes morphological evolution from (iv) a "cylindrical-like" shape to (v) a "dodecagonal" shape, ending with a thermodynamically stable (vi) "hexagonal" shape.

**Received:** October 24, 2014

**Revised:** January 12, 2015

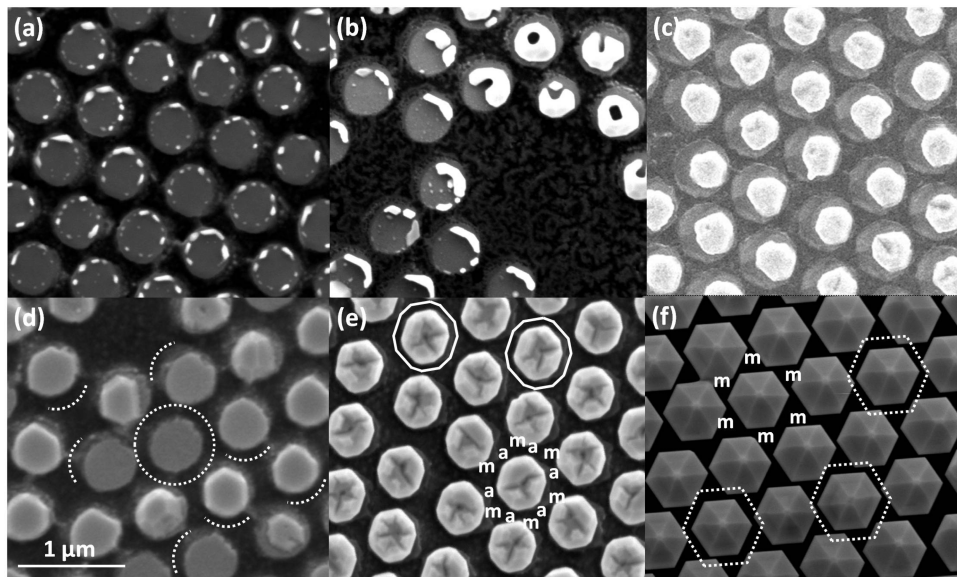


**Figure 1.** Top SEM view of samples A–C and D–F, corresponding to Stages I and II, respectively. Stage I: (a) (30 min) Nucleation; (b) (60 min) Coalescence onset; and (c) (90 min) Full coalescence. Stage II: (d) (120 min) Cylindrical-like shape; (e) (180 min) Dodecagonal shape; (f) (300 min) Hexagonal shape.

(i) Nucleation. In the initial growth stage, the Ga and N adatoms, impinge on the bare surface of the GaN substrate covered with a TiN nanohole mask. Under SAG conditions, GaN seeds nucleate exclusively within the nanoholes, preferentially along their inner perimeter, as shown in Figure 1a. During this nucleation step, their number (within a given nanohole) progressively increases until their density saturates.

(ii) Coalescence onset. By enlarging their size, the nucleation seeds start coalescing, forming a ringlike structure. This partially or fully closed ringlike structure, starts to grow toward the nanohole center, as shown in Figure 1b. The number of seeds (per given nanohole) progressively decreases until eventually a single GaN nanocrystal is formed (Figure 1b,c).

(iii) Full coalescence. The newly formed nanocrystal with still irregular shape (Figure 1c) continues to extend until it covers the entire nanohole area (Figure 1d). Note that the SAG conditions do not allow the GaN nanocrystal to extend further onto the mask surface.

(iv) Cylindrical-like shape. If SAG proceeds in a perfectly isotropic way within the nanohole, at the end of stage I the outer shell of the GaN nanocrystal should exhibit the shape of the underlying nanohole, that is, cylindrical (Figure 1d). However, a cylindrical shape imposed to a wurtzite nanocrystal is thermodynamically unstable, because it contains many energetically “high-cost” nonpolar facets. It is worth noticing that not all (but most) nanocrystals show a cylindrical shape (some show already distinct facets) because not all of them evolve simultaneously.

(v) Dodecagonal shape. The surface energy of *m*- and *a*-planes is lower than that of other nonpolar crystal planes.<sup>11–13</sup> Through the nanocrystal lateral growth, the free surface of these other nonpolar crystal planes is thus reduced (elimination of energetically “high-cost” planes) promoting the formation of *a*- and *m*-crystal facets. As a consequence, a dodecagonal 6*a*/6*m* nanocrystal is formed (Figure 1e).

(vi) Hexagonal shape. Being the surface energy of *m*-plane is somewhat lower than that of *a*-plane, the GaN nanocrystal continues its morphological evolution toward a thermodynamically stable hexagonal shape. Consequently, the free surface of energetically favorable *m*-facets gradually expands at the cost of the free surface of energetically less favorable *a*-facets (Figure 1e,f). Once the thermodynamically stable hexagonal (6*m*) shape is reached, the GaN nanocrystal ends its morphological evolution.

**Model for Growth Stage I.** Under the growth conditions that promote SAG, GaN nucleates exclusively within the nanoholes. Although the driving mechanisms for SAG are not precisely known, they are mainly attributed to different Ga adatom and/or GaN nuclei interaction with the two different underlying surfaces. Under steady-state growth conditions, the amorphous TiN surface and the crystalline GaN surface are at the same temperature. Weaker Ga adatom interactions with the amorphous TiN layer leads to a higher Ga desorption on TiN than on crystalline GaN. Similarly, an almost negligible GaN nuclei interaction with the amorphous TiN leads to a higher decomposition rate of GaN seeds that may form on TiN, compared to those formed on crystalline GaN. Consequently, for fixed impinging Ga and N fluxes there is a growth-temperature range (“growth window”) within which the GaN-on-GaN growth rate is positive (>0) whereas the GaN-on-TiN growth rate is zero (0), leading to the growth selectivity.

Similarly, weaker Ga adatom interaction with the amorphous TiN leads to a higher adatom diffusion on the mask in respect to that in the nanoholes. The discontinuity of diffusion coefficient introduces local diffusion currents on the sample surface resulting with a nonuniform concentration of Ga adatoms on it. Because of higher diffusion coefficient on TiN than on GaN, the Ga adatoms “escape” from the lithographic mask (nonpreferential nucleation domain), only to be “trapped” at the border of the nanoholes (preferential nucleation domain). The peripheral part of the nanohole thus behaves as the preferential area for initial nucleation of GaN, as experimentally observed (Figure 1a,b). This result is in a qualitative agreement with nucleation scenarios reported for different selective growth techniques of various III-nitride nanostructures.<sup>24–26</sup> These reports indicated the periphery of

the preferential nucleation domain (next to discontinuity region) as the preferential area for initial nucleation.

**Model for Growth Stage II.** Despite the condition of growth selectivity, the final NW size slightly surpasses the size of the underlying nanohole. This is not due to a GaN nucleation on the mask, which is hindered by the SAG kinetics, but due to the NW morphological evolution toward the shape that minimizes its total free energy per unit volume.<sup>23</sup>

A nanocrystal is composed of atoms, which, as a function of their energy, can be roughly divided into four different groups:

(i) bulk atoms, located inside the nanocrystal;

(ii) interface atoms, located at or close to the underlying interface;

(iii) surface atoms, located at or close to the free crystal facets;

(iv) edge atoms, located at or close to the crystal edges.

If the total energy per unit volume of an infinite, defect- and strain-free GaN crystal is taken as a reference ( $E_{\text{bulk}}^0 = 0$ ), the local energy of atoms may be altered due to either strain or proximity to the crystal boundaries, interface, surfaces, or edges. The total free-energy per unit volume of a growing nanocrystal can be written as<sup>23</sup>

$$E_{\text{total}} = E_{\text{strain}} + E_{\text{interface}} + E_{\text{surface}} + E_{\text{edge}} \quad (1)$$

The difference in total free energy of two distinct morphologies is likely the driving mechanism for shape transition, that is  $E_{\text{total}}(\text{cylindrical}) > E_{\text{total}}(\text{dodecagonal}) > E_{\text{total}}(\text{hexagonal})$ . Among the four terms contributing to  $E_{\text{total}}$  in eq 1, the energetically dominant term will drive the observed shape transitions.

Since the SAG proceeds homoepitaxially, yielding strain-free nanocrystals, the interface between the GaN NWs and the GaN substrate does not store free energy, that is,  $E_{\text{strain}} = E_{\text{interface}} = 0$ . In addition, the free surface energy per unit volume of a growing nanocrystal (with diameter  $d$  and total volume  $V$ ) is proportional to the total area of its free surface ( $S$ ):  $E_{\text{surface}} \sim S \cdot (1/V) \sim (1/d)$ . Similarly, the total edge energy per unit volume is proportional to the total length of its edges ( $L$ ):  $E_{\text{edge}} \sim L \cdot (1/V) \sim (1/d^2)$ . By increasing the crystal diameter ( $d \nearrow$ ) the contribution of the edge energy vanishes in respect to that of the free-surface energy. In a recent work on nucleation and morphological evolution of SA GaN NWs grown on amorphous SiN, Consonni et al. suggested strain and free-surface energy interplays as the driving mechanism for a spherical cap to a hexagonal prism shape transition. The authors also pointed out that for very small cap radii (around 5 nm) the contribution of the edge energy can be significant and comparable to those of strain and surface energy. However, in the present case the NWs have nearly 2 orders of magnitude larger diameter ( $\sim 500$  nm), implying that the contribution of the edge energy can be neglected in respect to the free-surface one. A hierarchy in the magnitude of the contributing energy terms for the considered nanocrystal is thus defined as

$$E_{\text{surface}} \gg E_{\text{edge}} > E_{\text{interface}} = E_{\text{strain}} = 0 \quad (2)$$

yielding:

$$E_{\text{total}} \approx E_{\text{surface}} = \frac{1}{V} \sum_j \gamma_j S_j \quad (3)$$

where  $\gamma_j$  and  $S_j$  are the surface energy per unit area of the  $j$ th crystal facet and its corresponding area, respectively.

At the onset of growth stage II, the GaN nanocrystal starts its morphological evolution from a cylindrical-like outer shell, which contains virtually all nonpolar crystal orientations, toward the energetically favorable dodecagonal and hexagonal shapes (Figures 2 and 3a). Figure 3b depicts the  $\gamma$  values of the

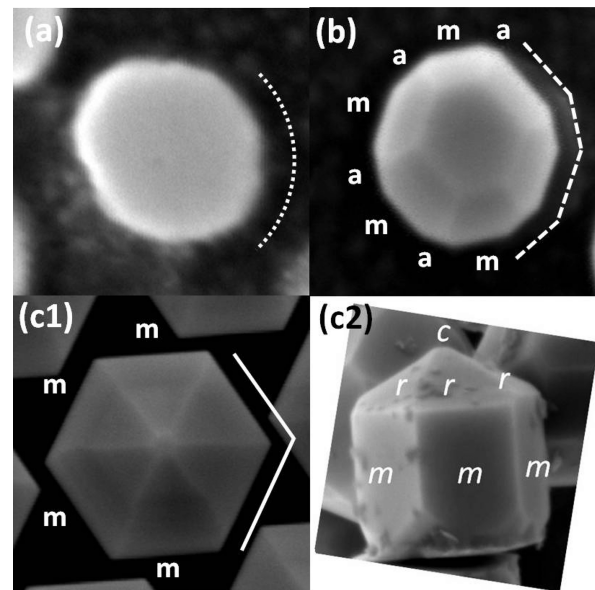


**Figure 2.** Stage II. SEM view of (a) cylindrical-like, (b) dodecagonal, and (c1–c2) hexagonal shape. The crystal facets are designated for clarity.

GaN nanocrystal outer shell, as a function of its shape and rotational coordinate  $\varphi$ .<sup>12</sup> Note that the  $\gamma(\varphi)$  function is featured only over 0 to 60° domain due to its 6-fold periodicity. The periodicity is a direct consequence of the spatial 6-fold symmetry of the hexagonal GaN crystal.

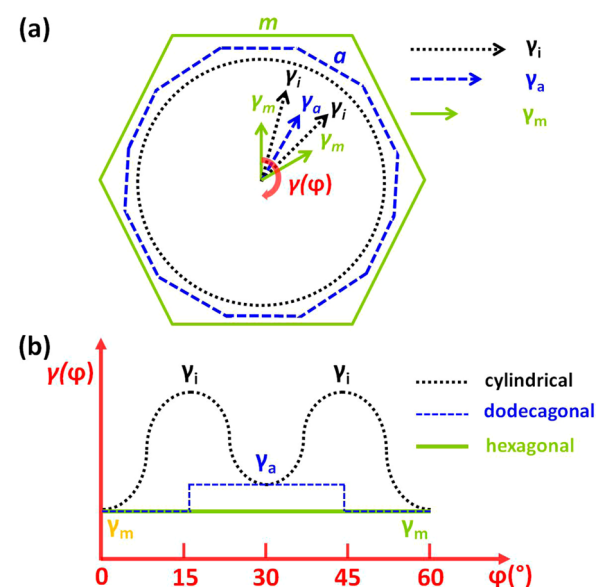


**Figure 3.** (a) Schematic presentation of the nanocrystal outer shell morphological evolution: cylindrical-like, dodecagonal (6a/6) and hexagonal (6m) shape. (b) As the morphological evolution proceeds, the  $\gamma(\varphi)$  evolves from an initial sine-wavelike function to an intermediate steplike function, finishing as a constant function.

Over the full  $\varphi$ -domain (0 to 360°), the  $\gamma(\varphi)$  function has 12 local minima, 6 of them in the direction of  $m$ -planes, labeled as  $\gamma_m$  ( $\varphi_m = 0^\circ + k \cdot 60^\circ$ ,  $k = 0, 1, \dots, 5$ ) and 6 of them in the direction of  $a$ -planes, labeled as  $\gamma_a$  ( $\varphi_a = 30^\circ + k \cdot 60^\circ$ ,  $k = 0, 1, \dots, 5$ ).<sup>12</sup> The function also has 12 local maxima. The crystal planes at which  $\gamma(\varphi)$  maximizes (the energetically “most costly” nonpolar facets) are labeled as intermediate  $i$ -planes, being the corresponding function maxima labeled as  $\gamma_i$  ( $\varphi_i \sim 15^\circ + k \cdot 30^\circ$ ,  $k = 0, 1, \dots, 11$ , see Figure 3a,b, for clarity).<sup>12</sup>

The existence of 12 local maxima of  $\gamma(\varphi)$  is identified as the driving mechanism for the appearance of dodecagonal crystal shape. Namely, the fact that  $\gamma(\varphi)$  function has its maxima in 12 crystal directions implies that the initial cylindrical-like nanocrystal will tend to minimize the free surface of energetically “high-cost”  $i$ -facets, by means of a faster growth rate along these 12 directions (in respect to other nonpolar directions), leading to the dodecagonalization ( $6a/6m$  shape) of the outer nanocrystal shell (Figures 2 and 3). Similarly, the existence of six minima of the  $\gamma(\varphi)$  function is identified as the driving mechanism for the formation of hexagonal crystal shape being the formation of free  $m$ -facets energetically preferential in respect to free  $a$ -facets ( $\gamma_m < \gamma_a$ ),<sup>11–13</sup> the GaN nanocrystal continues its evolution from the  $6a/6$  dodecagonal to the  $6m$  hexagonal form (Figures 2 and 3).

In both cases of SA GaN NWs grown on (i) thin amorphous SiN layer and (ii) thin AlN buffer layers on Si(111) substrates,<sup>21</sup> the authors reported that the nucleation is initiated in the form of spherical GaN caps. In the former case, the nucleation is characterized by a weak GaN-to-SiN epitaxial constraint whereas in the latter case, it is characterized by a strong GaN-to-AlN epitaxial constraint. The epitaxial constraint, together with a plastic relaxation (by dislocation formation) was suggested as the driving mechanism for the observed morphological evolution. In the former GaN-on-SiN case, the evolution follows two-step: (i) spherical cap to (ii) hexagonal NW transition. In the latter GaN-on-AlN case, two intermediate shapes have been observed, yielding the following four-step: (i) spherical cap to (ii) truncated hexagonal pyramid to (iii) full hexagonal pyramid to (iv) hexagonal NW transition. It was also suggested that in the case of self-nucleated GaN NWs both their diameter and shape evolution are determined by the energy interplays between strain, surface, and edge contributing terms (eq 1).

In contrast, the diameter of SAG GaN NWs is not determined in a self-nucleation process, but fixed by that of the TiN mask nanoholes and facilitated by the SAG kinetics. At the end of stage I, the GaN nanocrystal exhibits a cylindrical-like shape, which is imposed by the underlying circular nanohole. Because the cylindrical shape is incompatible with the total free-energy per unit-volume minimization criterion, the nanocrystal undergoes a further morphological evolution. In the present case of a (i) relatively big, (ii) homoepitaxially grown, and (iii) strain-free nanocrystal, its shape evolution is actually driven by the free-surface per unit-volume energy term exclusively. The consequences of the previous conditions are appearance of two thermodynamically unstable crystal shapes, a cylindrical-like and dodecagonal one, neither of which is observed in the case of SA GaN NWs.

In summary, we show that the formation of SAG GaN NWs proceeds in two stages, driven by SAG kinetics and free-surface-energy minimization, respectively. The first growth stage consists of the following three steps: initial nucleation at the nanohole inner periphery (driven by Ga adatom diffusion on a

discontinuous surface), coalescence onset, and full coalescence, finishing when the growing nanocrystal fills the entire nanohole area. In the second growth stage, the nanocrystal undergoes morphological evolution through unstable cylindrical-like and dodecagonal shapes, ending when the thermodynamically stable hexagonal NW is formed. The detailed understanding of the SAG GaN NWs formation opens the door for their further exploitation as “crystal platforms” for a wide variety of site-controlled III-N nanostructures.

## ■ AUTHOR INFORMATION

### Corresponding Author

\*E-mail: gacevic@isom.upm.es.

### Notes

The authors declare no competing financial interest.

## ■ ACKNOWLEDGMENTS

Z.G. thanks Dr. Liverios Lymperakis for critical reading of the manuscript. This work was partially supported by research grant EU FP7 Contract No. GECCO 280694-2.

## ■ REFERENCES

- (1) Yoshizawa, M.; Kikuchi, A.; Mori, M.; Fujita, N.; Kishino, K. *Jpn. J. Appl. Phys.* **1997**, *36*, L459.
- (2) Sánchez-García, M. A.; Calleja, E.; Monroy, E.; Sánchez, F. J.; Calle, F.; Muñoz, E.; Beresford, R. J. *J. Cryst. Growth* **1998**, *183*, 23.
- (3) Sekiguchi, H.; Kishino, K.; Kikuchi, A. *Appl. Phys. Express* **2008**, *1*, 124002.
- (4) Kishino, K.; Sekiguchi, H.; Kikuchi, A. *J. Cryst. Growth* **2009**, *311*, 2063.
- (5) Bengoechea-Encabo, A.; Barbagini, F.; Fernández-Garrido, S.; Grandal, J.; Ristić, J.; Sánchez-García, M. A.; Calleja, E.; Jahn, U.; Luna, E.; Trampert, A. *J. Cryst. Growth* **2011**, *325*, 89.
- (6) Gačević Ž.; Bengoechea-Encabo A.; Albert S.; Torres-Pardo A.; González-Calbet J. M.; Calleja E. *J. Appl. Phys.*, **2015**, *117*, 035301.
- (7) Sekiguchi, H.; Kishino, K.; Kikuchi, A. *Appl. Phys. Lett.* **2010**, *96*, 231104.
- (8) Holmes, M. J.; Choi, K.; Kako, S.; Arita, M.; Arakawa, Y. *Nano Lett.* **2014**, *14*, 982.
- (9) Matsubara, H.; Yoshimoto, S.; Saito, H.; Jianglin, Y.; Tanaka, Y.; Noda, S. *Science* **2008**, *319*, 445.
- (10) Kuhn, K. *J. Microelectron. Eng.* **2011**, *88*, 1044.
- (11) Northrup, J. E.; Neugebauer, J. *Phys. Rev. B* **1996**, *53*, R10477.
- (12) Jindal, V.; Shahedipour-Sandvik, F. *J. Appl. Phys.* **2009**, *106*, 083115.
- (13) Dreyer, C. E.; Janotti, A.; Van de Walle, C. G. *Phys. Rev. B* **2014**, *89*, 081305(R).
- (14) Deshpande, S.; Das, A.; Bhattacharya, P. *Appl. Phys. Lett.* **2013**, *102*, 161114.
- (15) Chernysheva E.; Lazić S.; Gačević Ž.; García-Lepetit N.; van der Meulen H. P.; Müller M.; Bertram F.; Veit P.; Torres-Pardo A.; González Calbet J. M.; Christen J.; Calleja E.; Calleja M. To be submitted for publication.
- (16) Ristić, J.; Calleja, E.; Sánchez-García, M. A.; Ulloa, J. M.; Sánchez-Páramo, J.; Calleja, J. M.; Jahn, U.; Trampert, A.; Ploog, K. H. *Phys. Rev. B* **2003**, *68*, 125305.
- (17) Albert, S.; Bengoechea-Encabo, A.; Lefebvre, P.; Barbagini, F.; Sánchez-García, M. A.; Calleja, E.; Jahn, U.; Trampert, A. *Appl. Phys. Lett.* **2012**, *100*, 231906.
- (18) Arbiol, J.; Magen, C.; Becker, P.; Jacopin, G.; Chernikov, A.; Schäfer, S.; Furtmayr, F.; Tchernycheva, M.; Rigutti, L.; Teubert, J.; Chatterjee, S.; Morante, J. R.; Eickhoff, M. *Nanoscale* **2012**, *4*, 7517.
- (19) Koester, R.; Hwang, J.-S.; Salomon, D.; Chen, X.; Bougerol, C.; Barnes, J.-P.; Le Si Dang, D.; Rigutti, L.; de Luna Bugallo, A.; Jacopin, G.; Tchernycheva, M.; Durand, C.; Eymery, J. *Nano Lett.* **2011**, *11*, 4839.

- (20) Consonni, V.; Hanke, M.; Knelangen, M.; Geelhaar, L.; Trampert, A.; Riechert, H. *Phys. Rev. B* **2011**, *83*, 035310.
- (21) Consonni, V.; Knelangen, M.; Geelhaar, L.; Trampert, A.; Riechert, H. *Phys. Rev. B* **2010**, *81*, 085310.
- (22) Bengoechea-Encabo, A.; Albert, S.; Sanchez-Garcia, M. A.; López, L. L.; Estradé, S.; Rebled, J. M.; Peiró, F.; Nataf, G.; de Mierry, P.; Zuniga-Perez, J.; Calleja, E. *J. Cryst. Growth* **2012**, *353*, 1.
- (23) Shchukin, V. A.; Bimberg, D. *Rev. Mod. Phys.* **1999**, *71*, 1125.
- (24) Ishizawa, S.; Sekiguchi, H.; Kikuchi, A.; Kishino, K. *Phys. Status Solidi B* **2007**, *244*, 1815.
- (25) Schumann, T.; Gotschke, T.; Limbach, F.; Stoica, T.; Calarco, R. *Nanotechnology* **2011**, *22*, 095603.
- (26) Winden, A.; Mikulics, M.; Stoica, T.; Von Der Ahe, M.; Mussler, G.; Haab, A.; Grützmacher, D.; Hardtdegen, H. *J. Cryst. Growth* **2013**, *370*, 336.